Sustainability in Environment
ISSN 2470-637X (Print) ISSN 2470-6388 (Online)
Vol. 11, No. 2, 2026
www.scholink.org/ojs/index.php/se

Original Paper

Study on Ecosystem Regulating Services in Karst World Heritage Based on Partial Correlation Analysis

Qingqing Xie[1], Kangning Xiong[1*], Yating Mu[1], & Qian Zhai[1]

[1] School of Karst Science, Guizhou Normal University/State Engineering Technology Institute for Karst Desertification Control, Guiyang 550001, Guizhou, China

[*] Corresponding Author

Received: February 01, 2026 Accepted: March 12, 2026 Online Published: March 23, 2026

doi:10.22158/se.v12n1p129 URL: http://dx.doi.org/10.22158/se.v12n1p129

Abstract

Understanding the spatiotemporal dynamics and interactions of ecosystem regulating services (ERSs) is crucial for safeguarding ecological security in karst world heritage (KWH) sites. Each KWH comprises two functional zones: the heritage site and the buffer zone. This study quantified three key ERSs—water conservation (WC), soil retention (SR), and carbon sequestration (CS)—from 2000 to 2020 within China's Shibing and Libo-Huanjiang KWHs. Results showed increases in SR and CS but a decrease in WC; heritage sites exhibited higher WC and SR but lower CS compared to buffer zones, with WC-CS hotspots located in buffer zones and SR hotspots in heritage sites. Slope, DEM, and mean annual temperature drove ERSs in Shibing, while slope, soil bulk density, and annual precipitation dominated those in Libo-Huanjiang. Strong WC-SR synergies occurred in buffer zones, accompanied by weak SR-CS and WC-CS tradeoffs, with heritage sites showing more pronounced weak SR-CS tradeoffs but fewer WC-CS tradeoffs than buffer zones. This research clarifies the spatiotemporal drivers of ERSs and their interactions, proposes a "heritage site-buffer zone" framework for tradeoff management, and provides a scientific basis for enhanced conservation.

Keywords

ecosystem regulating services, partial correlation analysis, karst world heritage sites, trade-off/synergy, influencing factor

1. Introduction

Ecosystem services (ESs) refer to the diverse products and services that ecosystems provide to humans, directly or indirectly, to enable them to sustain their survival and development (Costanza et al., 1997). According to the classification framework of the Millennium Ecosystem Assessment, ESs are

categorised into four major types: regulating services, provisioning services, supporting services, and cultural services (Zhang et al., 2021). Among these, ecosystem regulating services (ERSs) safeguard ecological security through invisible mechanisms such as mitigating climate change and regulating hydrology. In the practice of ESs conservation and assessment, the public good attributes of ERSs mean they are often undervalued or even overlooked compared to provisioning services possessing direct economic value (Carpenter, 2006). This phenomenon is particularly pronounced in ecologically fragile regions. For instance, in karst areas, the erosion of rock formations may lead to a decline in ERSs, potentially triggering irreversible ecological degradation.

Karst World Heritage (KWH) comprises Karst World Heritage Sites (heritage sites) and their buffer zones. As vital providers of ecosystem services, KWH encompasses a combined land and marine area of 296 million hectares, which accounts for approximately 8% of the world's total protected areas (Fang et al., 2024). Among these, the South China Karst constitutes the largest cluster of karst-type heritage sites worldwide. They not only harbour typical tropical and subtropical karst ecosystems but also feature unparalleled combinations of karst landforms (Zhang et al., 2022), such as the sword-shaped and tower-shaped karst formations in Yunnan's Stone Forest, conical karst in Libo, canyon karst in Wulong, and dolomite karst in Shibing. These heritage sites provide a complete record of the geological evolutionary sequence and key processes of tropical-subtropical karst landforms on Earth, serving as a vital natural specimen for studying global karst evolution (UNESCO World Heritage Centre, Operational Guidelines for the Implementation of the World Heritage Convention. WHC.21/01, 2021). The Outstanding Universal Value (OUV) of these sites is rooted not only in the exceptional aesthetic value of their landscapes—shaped by unique and representative karst topography—and their significant geological and ecological importance (Zhao, Xiong, & Zhang, 2024), but also relies heavily on the stable provision of ERSs (Huang et al., 2024). Given karst's inherent environmental characteristics of high rock exposure, shallow soils, and significant groundwater leakage (Zhang et al., 2021), these ERSs provide critical support for the long-term sustainability of the site's landscape-ecosystem complex by maintaining the structural integrity, functional stability, and process continuity of karst ecosystems (Liu, Lian, & Chen, 2024). However, the inherent fragility, sensitivity, and low natural resilience of karst environments (Xiong, Li, & Wang, 2012) render their ERSs highly responsive to climate change and human activities (He, Zhao, & Yu, 2021). Consequently, research into the ERSs of KWH holds significant scientific and practical value (Gong, Yin, & Chen, 2023). It is essential for maintaining the ecological security barrier function of these sites, ensuring the sustainable use of regional natural resources, and ultimately supporting the conservation and management of global karst ecosystems.

Among the methodological approaches for assessing trade-offs and synergies among ecosystem services, correlation analysis represents one of the most commonly employed techniques, primarily encompassing Spearman rank correlation and Pearson linear correlation analysis (Chang, Zhang, & Yao, 2026). Spearman correlation analysis examines the association between rank orders of time-series data

without requiring strict linear relationships between variables (Zhang et al., 2025). This method effectively circumvents the interference of non-linear dynamic characteristics exhibited by ecosystem services in the temporal dimension due to climate fluctuations, land use transitions, and other factors (Wang et al., 2025), thereby better revealing the temporal evolution patterns of trade-off and synergy relationships among ecosystem regulating services in karst heritage sites. However, Spearman correlation analysis is primarily applicable for identifying trade-off and synergy relationships among ecosystem services along time series, with relatively limited capacity for expressing spatial heterogeneity (Chang, Zhang, & Yao, 2026). In contrast, partial correlation analysis can effectively eliminate the interference of irrelevant factors (Chang, Zhang, & Yao, 2026). While more clearly explaining the dynamic changes of trade-off and synergy relationships along the time series, it can also reveal statistically significant differences in space, thereby enhancing the reliability of research findings (Xia & Huang, 2025). Unlike ordinary correlation analysis, partial correlation analysis controls for other potential confounding variables (such as topographic conditions, climatic factors, and human activity intensity), effectively isolating the net correlation between two ecosystem services and accurately identifying the intrinsic interaction mechanisms among different ecosystem services (Jiang, et al., 2025). This method offers advantages including a concise theoretical foundation, standardized operational procedures, and intuitive result presentation, making it suitable for quantifying trade-off and synergy relationships among multiple ecosystem services in complex karst heritage sites.

Current research on KWHs predominantly focuses on landscape aesthetic evaluation, landscape stability, and conservation-tourism synergies (Zhang et al., 2023; Bai et al., 2024). In recent years, as research on ERSs has deepened, scholars have begun to focus on this field within KWHs. For instance, Chen et al. (2024) employed spatial overlay methods to identify spatial differentiation characteristics of trade-off/synergy relationships, and compared ERSs between karst and non-karst heritage sites. Feng et al. (2024) adopted a holistic approach to investigate trade-off/synergy relationships and spatial scale effects in KWHs' ERSs across three time periods: 2000, 2010, and 2020. Although research on ERSs in KWHs has made some progress, existing studies predominantly focus on the sites as a whole, with insufficient attention paid to the ecological differences between heritage sites and buffer zones. Understanding of trade-offs/synergies among ERSs remains incomplete, particularly lacking in-depth research on their spatio-temporal differentiation. Consequently, urgent research is needed on the spatio-temporal variation, drivers, and trade-off/synergy relationships of ERSs in KWHs.

This study takes the Shibing KWH and the Libo-Huanjiang KWH (hereafter referred to as Shibing and Libo-Huanjiang) as case studies. The InVEST model and empirical models were employed to assess and visualise three key ERSs within KWHs: water conservation (WC), soil retention (SR), and carbon sequestration (CS). Geodetector analysis was employed to examine the drivers of these ERSs, while Spearman correlation and partial correlation analyses were used to investigate trade-offs and synergies among them. The primary objectives of this study are: (1) to elucidate the spatiotemporal variation characteristics and key drivers of ERSs in KWHs over a long-term timescale; (2) to clarify the

trade-offs/synergies among ERSs in KWHs and establish a "heritage site-buffer zone" dual-zone regulatory framework for managing such interactions. This research aims to provide decision-making support for ecological conservation and sustainable resource utilisation in KWHs.

2. Materials and Methods

2.1 Study Areas

This study selects the Shibing Karst World Natural Heritage Site and the Libo-Huanjiang Karst World Natural Heritage Site as the research objects (Figure 1.). Shibing is located in the Qiandongnan Miao and Dong Autonomous Prefecture (central-eastern Guizhou Province), with geographical coordinates of 108°05′40″E and 27°10′16″N, covering a total area of 28,295 ha (10,280 ha for the heritage site and 18,015 ha for the buffer zone). Libo-Huanjiang is situated at the junction of Libo County (Qiannan Buyi and Miao Autonomous Prefecture, Guizhou Province) and Huanjiang Maonan Autonomous County (Hechi City, Guangxi Zhuang Autonomous Region), with coordinates of 107°58′30″E, 25°09′27″N–25°13′15″N, and a total study area of 84,575 ha (36,647 ha for the heritage site and 47,928 ha for the buffer zone).

As core and representative units of the South China Karst heritage system, Shibing and Libo-Huanjiang have unique characteristics and significant value in three key dimensions, which are the core reasons for selecting them as research objects. In terms of geomorphological characteristics, both sites have remarkable scarcity and typicality: Shibing is a globally rare concentrated area of dolomitic karst landforms, with a complete combination of dolomitic karst landforms such as canyons, peak clusters and peak forests, filling the gap in the global study of dolomitic karst (Zhang et al., 2022); Libo-Huanjiang is a typical representative of conical karst, with high peak cluster density and well-developed depressions, forming an extreme landscape and ecological prototype of tropical-subtropical karst and reflecting the Outstanding Universal Value (OUV) of the heritage. In terms of ecological support, both are important water conservation areas of the Yangtze and Pearl River basins; their ecosystem regulating services not only maintain the structural integrity and functional stability of the karst ecosystem itself (Liu, Lian, & Chen, 2024) but also support the water security and agricultural production of millions of people downstream, serving as the core of the regional ecological security barrier. In terms of heritage value, the OUV of both sites relies not only on the landscape aesthetic value shaped by unique karst landforms (Zhao, Xiong, & Zhang, 2024) but also on the stable supply of ecosystem regulating services; the degradation of regulating services will directly threaten the integrity and survival of heritage value (Huang et al., 2024).

However, Shibing and Libo-Huanjiang are facing severe ecological challenges. Frequent extreme weather events caused by global climate change have intensified the instability of the karst ecosystem, leading to fluctuating water conservation capacity and increased soil erosion risks (He, Zhao, & Yu, 2021). Meanwhile, the increasing intensity of human activities such as agricultural production and tourism development around the heritage sites has disturbed surface vegetation and hydrological

processes, which may disrupt the balance of regulating services. Coupled with the inherent high vulnerability and low resilience of the karst ecosystem, the degradation of regulating services is irreversible, threatening the heritage security and downstream ecological balance. Therefore, studying ecosystem regulating services in these two sites is of great scientific and practical significance for maintaining heritage ecological security, ensuring the sustainable use of regional resources, and supporting global karst ecological governance.

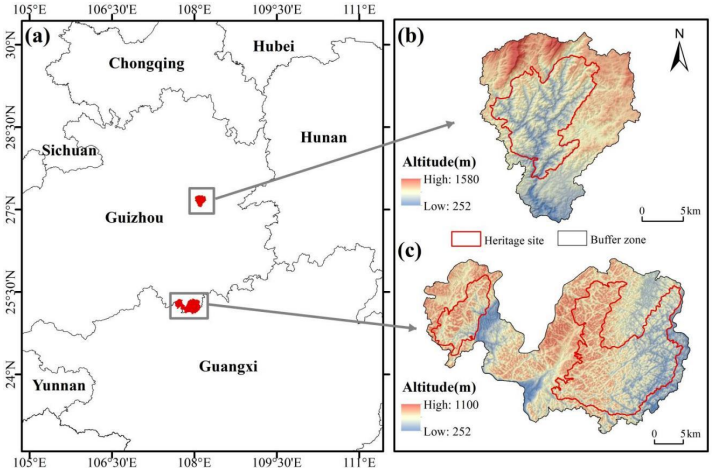

Figure 1. Study areas. (a) Location of Study Areas. (b) Shibing Karst Heritage. (c) Libo-Huanjiang Karst Heritage

2.2 Data Sources

In accordance with the research objectives, this study utilised a wide range of data sources (Table 1). To minimise errors arising from spatial resolution and coordinate system discrepancies, all data were uniformly projected into WGS_1984_UTM_Zone_49N within ArcMap 10.8, with a standardised spatial resolution of 30 metres.

Table 1. Data Sources

Data	Resolution	Type	Source
Digital Elevation Model (DEM)	12.5m	Raster	https://search.earthdata.nasa.gov/search
Net Primary Production (NPP)	250m	Raster	https://www.usgs.gov
Leaf Area Index (LAI)	500m	Raster	https://earthengine.google.com
Land Use and Land Cover Data (LULC)	30m	Raster	https://earthexplorer.usgs.gov/
Normalized Difference Vegetation Index (NDVI)	30m	Raster	http://www.nesdc.org.cn/
Soil Type Sand, silt, clay, soil organic carbon	250m	Raster	https://www.tpdc.ac.cn

(OC), soil pH (PH), soil bulk density(BD)			
Meteorological data			
Relative humidity (RH), annual precipitation (AP), mean annual temperature (MAT), potential evapotranspiration	1000m	Raster	https://www.tpdc.ac.cn
Road density (RD)	-	Vector	https://download.geofabrik.de
Gross Domestic Product (GDP)	-	Vector	Statistical Yearbook
Population Density (PD)	-	Vector	Statistical Yearbook

2.3 Research Methodology

2.3.1 ERSs Assessment

Drawing on research findings regarding ecosystem services in karst heritage sites [21], this study selected three regulating services: water conservation (WC), soil retention (SR), and carbon sequestration (CS) (Table 2).

Table 2. Methods for Quantifying ERSs

Types	Evaluation methodology
WC	The InVEST(Integrated Valuation of Ecosystem Services and Trade-offs) Water Yield module was used to calculate pixel-level water yield based on the water balance equation [20], followed by the quantification of WC capacity. The specific calculation formula is as follows: $$WR = Min\left(1, \frac{249}{V}\right) \times Min\left(1, \frac{0.9 \times TI}{3}\right) \times Min\left(1, \frac{K}{300}\right) \times Y \quad (1)$$ Where: WR denotes water conservation volume (mm) in the study area; V represents the flow velocity coefficient; K signifies the saturated hydraulic conductivity of the soil; Y indicates water yield; TI denotes the topographic index.
SR	The InVEST Sediment Delivery Ratio (SDR) module was used to calculate SR, employing the Universal Soil Loss Equation [21]. The specific formula is presented below: $$RKLS_i = R_i \times K_i \times LS_i \quad (2)$$ $$USLE_i = R_i \times K_i \times LS_i \times C_i \times P_i \quad (3)$$ $$SEDRET_i = RKLS_i - USLE_i \quad (4)$$ Where: RKLSi denotes potential soil erosion, measured in tonnes per hectare; USLEi

	denotes actual erosion, measured in tonnes per hectare; Ri denotes rainfall erosion strength factor; Ki denotes soil erodibility factor; LSi denotes slope length and gradient factor; Ci denotes the cover and management factor; Pi denotes the soil conservation measure factor; SEDRETi represents the SR amount in the study area; RKLSi - USLEi represents the sediment retention amount in the study area.
CS	Net primary productivity (NPP) represents the organic matter produced by vegetation. Based on the principle that vegetation can sequester 1.63 kg of carbon dioxide during the accumulation of 1 kg of NPP [22], the calculation formula is: $$C_i = 1.63 \times NPP_i \quad (5)$$ Where: Ci denotes CS amount of the per grid cell, measured in g/m²; NPPi denotes the net primary productivity of grid cell i, measured in g/m2.

2.3.2 Spatial Statistical Analysis

Grids of 30, 50, 100, 250, and 500 metres were examined to determine the optimal characteristic scale. Ultimately, a 100m × 100m grid scale was adopted. Spatial autocorrelation analysis was employed to explore the spatial relationships between ERS change rates and surrounding factors. The Getis-Ord Gi* statistic was further applied to reveal spatial distribution patterns of ERS hotspots (high-value clusters) and coldspots (low-value clusters) across KWHSs. The calculation formula is:

$$Getis-Ord\ G_i^* = \frac{\sum_{j=1}^{n} w_{ij}x_j - X\sum_{j=1}^{n} w_{ij}x_j}{\sqrt{[n\sum_{j=1}^{n} w_{ij}^2 - (\sum_{j=1}^{n} w_{ij})^2]/(n-1)}} \quad (6)$$

where n denotes the number of grids in the study area; xi and xj represent ecosystem services in grid i and j respectively; is the mean ecosystem service value; and wij is the spatial weight matrix constructed between grids i and j.

2.3.3 Geodetector Analysis

Based on the current status of KWHs, data availability, representativeness, and prior research, this study selected topographic (slope, aspect, DEM), climatic (AP, MAT, RH), vegetation (LAI, NDVI), soil (BD, PH, OC), and anthropogenic (PD, GDP, RD) factors. All indicators were imported into ArcMap 10.8, with the Grid tool generating grid cells at different scales. After multiple iterative tests on sample points, the 100m × 100m grid yielded optimal Geodetector results (highest q-value). The “Extract Multi-Values to Points” tool was then used to obtain multi-period ERS values, which were set as the Y variable; the 14 drivers served as X variables for analysis via the “GD” package in R. The calculation formula is:

$$q = 1 - \frac{\sum_{h=1}^{L} N_h \sigma_h^2}{N\sigma^2} \tag{7}$$

where h denotes the stratum or partition of variable Y or factor X (h=1,…,L), Nh and N represent the number of cells in stratum h and the entire area respectively; $\sigma_h^2$and σ^2 represent thevariance of Y within layer h and across the entire area, respectively. The q value ranges from 0 to 1; a higher value indicates a more pronounced spatial differentiation of variable Y attributable to that factor. Specifically, if the stratification is generated by independent variable X, a larger q value signifies greater explanatory power of X over Y, while a smaller value indicates weaker explanatory power. When q=1, factor X fully controls the spatial distribution of Y; when q=0, no relationship exists between X and Y. The q-value indicates that X explains 100×q% of Y.

2.3.4 Trade-off and Synergy Analysis

This study used Spearman's correlation analysis to characterize temporal trade-off/synergy relationships between ERSs in KWHs. Values extracted from ArcMap 10.8 were analyzed via SPSS 27.0 for correlation and subsequent t-tests. A trade-off was identified if two ERSs passed the 0.05 significance test with a negative correlation coefficient; otherwise, a synergy was confirmed. Pixel-by-pixel partial correlation analysis was employed to explore spatial ERS trade-off/synergy relationships. This method eliminates confounding factors (Jiang et al., 2025), clarifies statistically significant spatial variations in ERSs (Li et al., 2024), and enhances result credibility. The calculation formula is as follows:

Step one: Calculation of correlation coefficients:

$$r_{12(ij)} = \frac{\sum_1^n (ES1_{n(ij)} - \overline{ES1_{n(ij)}})(ES2_{n(ij)} - \overline{ES2_{n(ij)}})}{\sqrt{\sum_1^n (ES1_{n(ij)} - \overline{ES1_{n(ij)}})^2 \sum_1^n (ES2_{n(ij)} - \overline{ES2_{n(ij)}})^2}} \tag{8}$$

Step 2: Calculate the first-order partial correlation coefficient

$$r_{12.3(ij)} = \frac{r_{12(ij)} - r_{13(ij)} r_{23(ij)}}{\sqrt{(1 - r_{13(ij)}^2)(1 - r_{23(ij)}^2)}} \tag{9}$$

Step 3: Calculate the second-order partial correlation coefficients

$$r_{12.34(ij)} = \frac{r_{12.3(ij)} - r_{14.3(ij)} r_{24.3(ij)}}{\sqrt{(1 - r_{14.3(ij)}^2)(1 - r_{24.3(ij)}^2)}} \tag{10}$$

Where: *ES1* and *ES2* represent two types of ERSs; *r* denotes the correlation coefficient between *ES1* and *ES2*; *i* and *j* denote the row and column indices of a grid cell, respectively; n denotes the time series of the grid data. $r_{12(ij)}$ represents the simple correlation coefficient between *ES1* and *ES2* at pixel *ij* in year *n*, assuming all other ERSs undergo changes. Similarly, we can derive: $r_{123(ij)}$, $r_{124(ij)}$ etc. represents the first-order partial correlation coefficient between *ES1* and *ES2* at pixel *ij* when one ERS

remains constant; $r_{12.34(ij)}$ represents the second-order partial correlation coefficient between *ES1* and *ES2* at pixel *ij* when other ERSs remain constant. Employing t-tests, we assess the significance of ERS interactions and classify them as follows: Strong synergy (Synergy**, r > 0, P < 0.05), Moderate Synergy (Synergy*, r > 0, 0.05 < P < 0.1), Weak Synergy (Synergy, r > 0, 0.1 < P*)*, Strong Trade-off (Trade-off**, r < 0, P < 0.05), Moderate trade-off (Trade-off*, r < 0, 0.05 < P < 0.1), Weak trade-off (Trade-off, r < 0, 0.1 < P*)*, and No relationship (r = 0).

Geodetector was employed for interaction detection with time-series data. Control variables for partial correlation analysis were selected by maximizing the q-value: in Shibing, NDVI and MAT for WC-SR, LAI and MAT for SR-CS and WC-CS; in Libo-Huanjiang, NDVI and AP for WC-SR, LAI and AP for SR-CS and WC-CS.

3. Results

3.1 Spatiotemporal Characteristics of ERSs

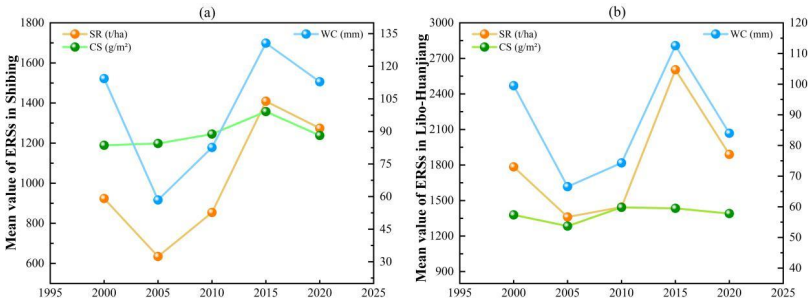

Figure 2. Temporal Changes in ERSs from 2000 to 2020 (a refers to Shibing, and b refers to Libo-Huanjiang)

On the temporal dimension, the mean values of the three ERSs in Shibing and Libo-Huanjiang exhibited no consistent increasing or decreasing trend during the period 2000–2020. Specifically, both study areas showed increasing trends in SR (with total growth rates of 37.93% and 5.91%, respectively) and CS (4.22% and 0.89%), whereas WC displayed decreasing trends (-1.27% and -15.60%) (Figure 2). Spatially, Shibing exhibited a “north-high/south-low and west-high/east-low” distribution pattern for SR and WC, while CS followed a “north-low/south-high” pattern. In Libo-Huanjiang, SR and WC values showed fluctuating trends from west to east, and CS exhibited a “west-high/east-low” distribution pattern (Figure 3). Regarding heritage site-buffer zone disparities across the two study areas, the mean WC value in heritage sites was slightly higher than that in buffer zones (with a difference ranging from 1.03% to 6.03%); the disparity in mean SR values was the most significant (heritage sites exceeded those in buffer zones by 9.85%–74.92%); and the mean CS value in heritage sites was lower than that in buffer zones (with a difference ranging from 0.24% to 27.55%).

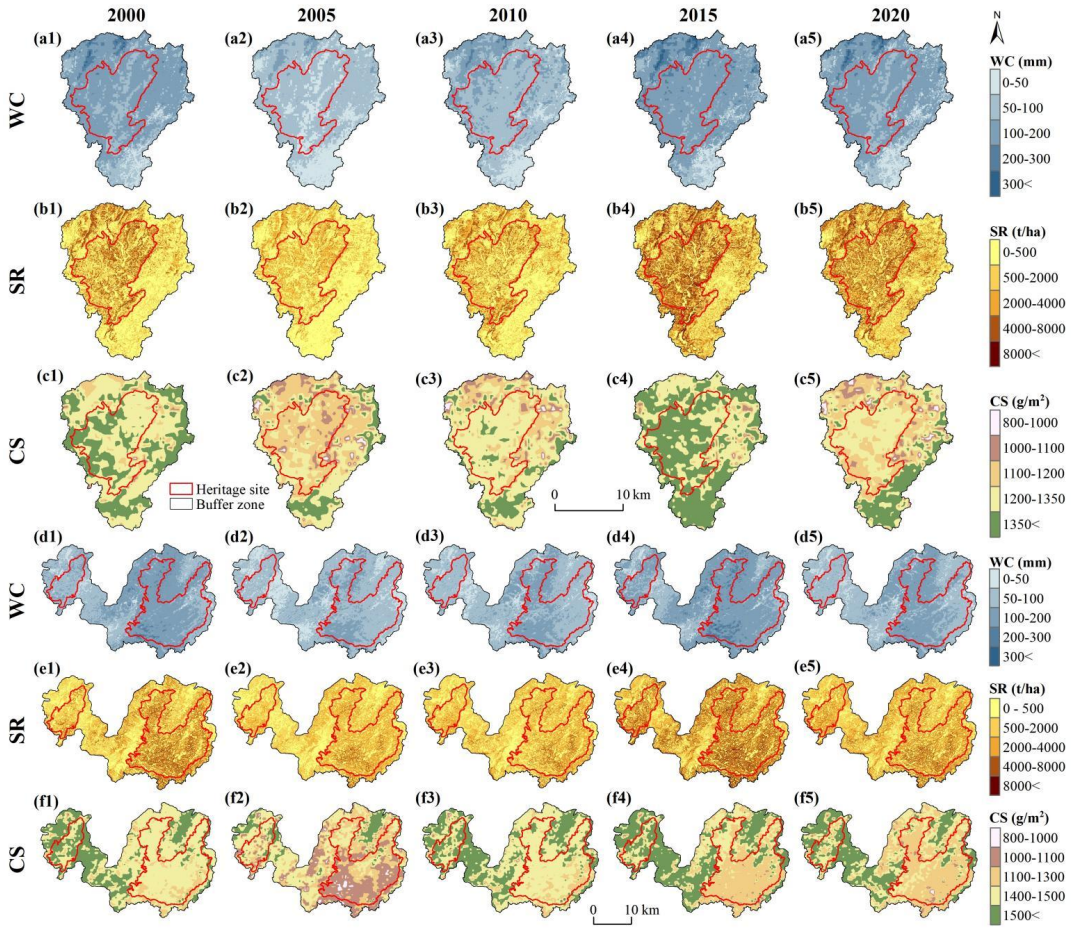

Figure 3. Spatial Distribution in ERSs from 2000 to 2020 (a1-c5 refer to Shibing, and d1-f5 refer to Libo-Huanjiang)

4.2 Spatial Distribution of Hotspots and Coldspots in ERSs

To capture the spatial clustering characteristics of the three ERSs in KWHs, hotspot analysis was conducted across Shibing and Libo-Huanjiang. Most regions showed no significant spatial pattern for all three ERSs, with SR hotspots and coldspots exhibiting the weakest clustering (Figure 4). In Shibing, the average proportions of WC and CS hotspots (11.19%, 17.54%) and coldspots (13.60%, 16.49%) in the buffer zone were higher than those in the heritage site over the 2000–2020 period. Only SR hotspots were more prevalent in the heritage site (9.77%) than in the buffer zone (6.44%) (Table 3). In Libo-Huanjiang, the proportions of WC and SR hotspots in the heritage site (10.86%, 11.82%) were significantly higher than those in the buffer zone (7.45%, 5.01%), while coldspots (5.41%, 3.90%) were lower (buffer zone: 11.27%, 13.89%). CS coldspots accounted for a significantly higher proportion in the heritage site (15.68%) than the buffer zone (8.63%), indicating low-value aggregation in the heritage site.

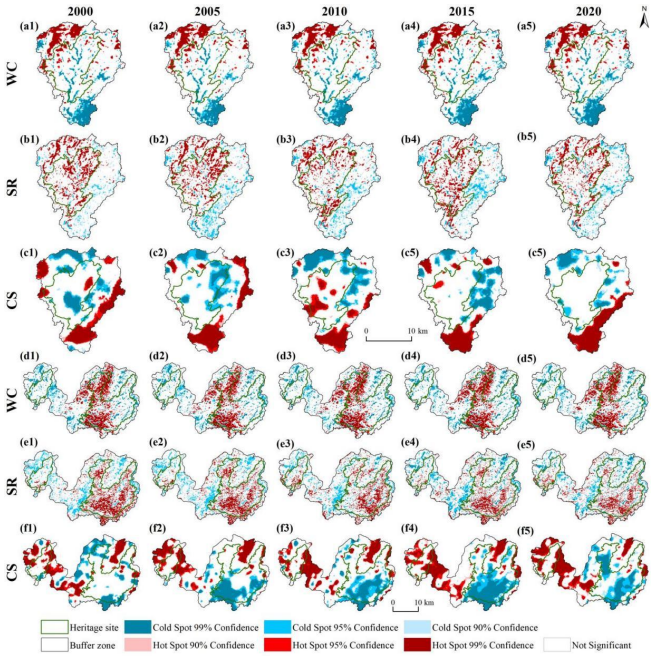

Figure 4. Spatial Distribution of Cold and Hot Spots of Ecosystem Regulating Services from 2000 to 2020 (a1-c5 refer to Shibing, and d1-f5 refer to Libo-Huanjiang)

Table 3. Annual Mean Proportion of Coldspots and Hotspots in ERSs (%)

Karst Heritage site	Zone Type	Proportion of hotspots			Proportion of coldspots		
		WC	SR	CS	WC	SR	CS
Shibing	Heritage site	3.20	9.77	2.41	4.35	1.60	5.92
	Buffer zone	11.19	6.44	17.54	13.60	11.87	16.49
Libo-Huanjiang	Heritage site	10.86	11.82	4.25	5.41	3.90	15.68
	Buffer zone	7.45	5.01	19.10	11.27	13.89	8.63

4.3 Spatial Distribution of Hotspots and Coldspots in ERSs

Table 4. Monitoring Results of Single Factors of Ecosystem Regulating Services

q value	Shibing			Libo-Huanjiang		
	SR	WC	CS	SR	WC	CS
X1	0.03***	0.08***	0.23*	0.05***	0.03***	0.21***
X2	0.05***	0.36***	0.32***	0.01***	0.12***	0.09***
X3	0.33***	0.17***	0.09***	0.21***	0.07***	0.04*
X4	0.03***	0.33***	0.19***	0.06***	0.23***	0.53***
X5	0.01*	0.05***	0.04*	0.01***	0.03***	0.19***
X6	0.03***	0.04**	0.01*	0.04***	0.05***	0.03*

X7	0.08***	0.05***	0.04*	0.06***	0.06***	0.18***
X8	0.03***	0.31***	0.08*	0.08***	0.24***	0.39***
X9	0.02***	0.20***	0.17***	0.07***	0.32***	0.30***
X10	0.02*	0.38***	0.09***	0.09***	0.38***	0.49***
X11	0.08***	0.08***	0.13*	0.07***	0.11***	0.46***
X12	0.38***	0.05***	0.02*	0.41***	0.14***	0.08***
X13	0.05***	0.40***	0.19*	0.03***	0.23***	0.05***
X14	0.02***	0.01**	0.01 ***	0.01***	0.01**	0.01*

Note. X1 denotes GDP; X2 denotes MAT; X3 denotes NDVI; X4 denotes AP; X5 denotes RH; X6 denotes RD; X7 denotes PD; X8 denotes OC; X9 denotes pH; X10 denotes BD; X11 denotes LAI; X12 denotes slope; X13 denotes DEM; X14 denotes aspect; *** indicates $p < 0.001$; ** indicates $p < 0.01$; * indicates $p < 0.05$.

Geodetector was used to investigate drivers of ERS spatiotemporal variations in Shibing and Libo-Huanjiang (Table 4). Each influencing factor exerted varying degrees of impact on the spatial distribution patterns of ERSs. In Shibing, slope (q=0.38) had high explanatory power for SR, being its primary determinant; DEM (q=0.40) dominated WC spatial patterns; MAT (q=0.32) was key for CS. In Libo-Huanjiang, slope (q=0.41) primarily influenced SR distribution; BD (q=0.38) was the main factor for WC; AP (q=0.53) dominated CS spatial patterns.

The explanatory power of two-factor interactions exceeded that of single-factor effects, with interactions categorized as dual-factor enhancement or non-linear enhancement. Non-linear enhancement dominated in Shibing, while dual-factor enhancement prevailed in Libo-Huanjiang (Figure 5). For SR, slope and NDVI showed the strongest interactive effects in both areas (q=0.63 and 0.55, respectively). For WC spatial distribution, key factor combinations were DEM and NDVI (q=0.54) in Shibing, and DEM and BD (q=0.44) in Libo-Huanjiang. For CS spatial distribution, LAI and TEM (q=0.57) in Shibing, and LAI and AR (q=0.67) in Libo-Huanjiang, exerted the most significant effects.

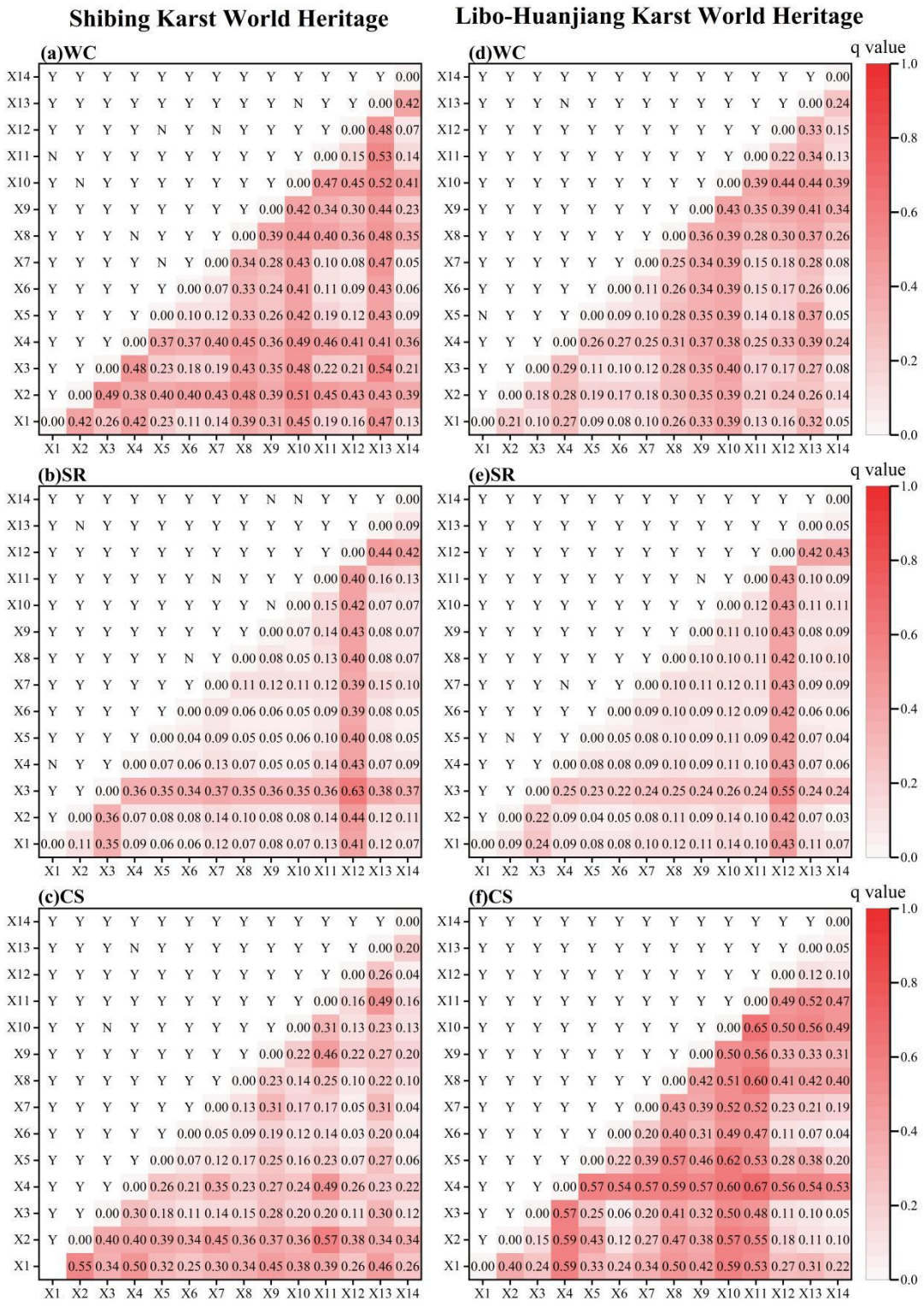

Figure 5. Monitoring Results of Interaction among Ecosystem Regulating Services (Note: a-c refer to Shibing; d-f refer to Libo-Huanjiang; X1 Denotes GDP; X2 Denotes MAT; X3 Denotes NDVI; X4 Denotes AP; X5 Denotes RH; X6 Denotes RD; X7 Denotes PD; X8 Denotes OC; X9 Denotes pH; X10 Denotes BD; X11 Denotes LAI; X12 Denotes Slope; X13 Denotes DEM; X14 Denotes Aspect;)

4.4 Trade-offs and Synergistic Relationships of ERSs

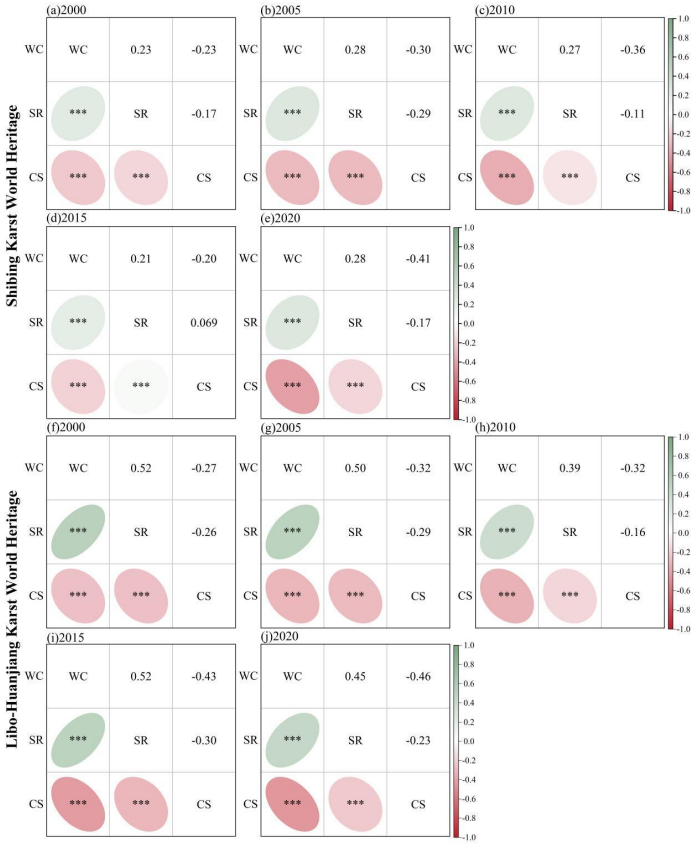

Figure 6. Results of Spearman Correlation Analysis on Ecosystem Regulating Services (a-e refer to Shibing, and f-j refer to Libo-Huanjiang)

Spearman's correlation analyses were performed for each pair of the three typical ERSs in Shibing and Libo-Huanjiang (2000-2020), with all results passing significance tests ($p \leq 0.001$) (Figure 6). During the study period, WC and SR showed synergies across both heritage sites, while WC-CS and SR-CS interactions were trade-offs-with WC-CS trade-off magnitude consistently higher than that of SR-CS. In Shibing, the WC-SR correlation coefficient remained stable (0.21-0.28), the absolute value of WC-CS correlation varied widely (0.2-0.41), and the absolute value of SR-CS negative correlation was unstable (0.069-0.29), indicating an overall weak association. In Libo-Huanjiang, the WC-SR correlation coefficient fluctuated between 0.39 and 0.52. The absolute value of WC-CS correlation increased from 0.27 in 2000 to 0.46 in 2020, while that of SR-CS correlation fluctuated between 0.16 and 0.30, showing an overall fluctuating upward trend.

Spatial trade-off/synergy relationships of ERSs were mapped using partial correlation analysis. Overall, these relationships were scattered without distinct clustering patterns (Figure 7, Table 5). In Shibing, there were no "unrelated" zones across all three service pairs (WC-SR, SR-CS, WC-CS), with synergies dominating. Strong synergies accounted for 18.66%-26.86% in the heritage site, compared to 29.38%-46.76% in the buffer zone. Libo-Huanjiang also had no "unrelated" ERS relationship zones,

but trade-off/synergy spatial differentiation was more pronounced. WC-SR was dominated by strong synergies, with the buffer zone (19.23%) having a higher proportion than the heritage site (17.38%). Both SR-CS and WC-CS had relatively high weak trade-off proportions: SR-CS weak trade-offs were higher in the heritage site (27.11%) than the buffer zone (25.28%), while WC-CS weak trade-offs were lower in the heritage site (21.84%) than the buffer zone (42.35%).

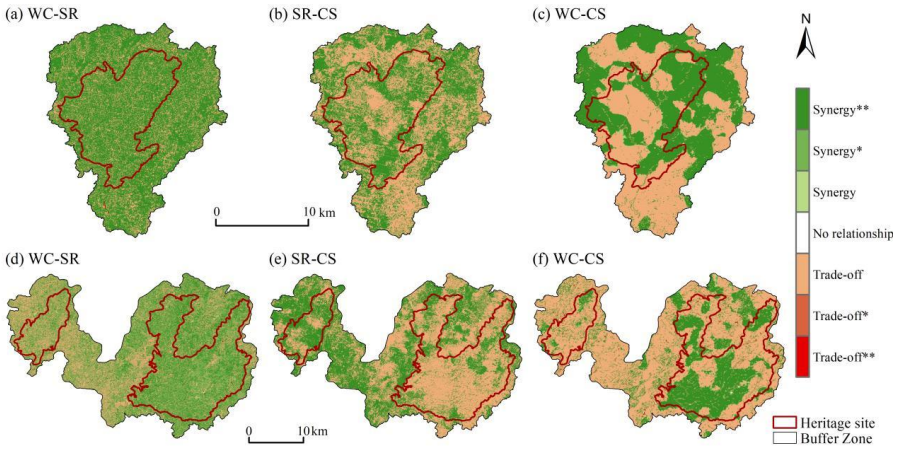

Figure 7. Results of Partial Correlation Analysis of ERSs (a-c refer to Shibing, and d-f refer to Libo-Huanjiang)

Table 5. Statistics on the Spatial Proportion of ERSs Trade-offs and Synergies

Karst World Heritage Site	Correlation Type	Heritage Site			Buffer Zone		
		WC-SR	SR-CS	WC-CS	WC-SR	SR-CS	WC-CS
Shibing	Trade-off**	0.01	0.00	0.01	0.05	0.00	0.00
	Trade-off*	0.00	0.00	0.00	0.00	0.00	0.00
	Trade-off	8.61	16.77	16.37	15.47	30.80	32.51
	No relationship	0.00	0.00	0.00	0.00	0.00	0.00
	Synergy	0.45	0.53	0.62	0.72	0.97	0.88
	Synergy*	0.40	0.55	0.61	0.68	0.95	0.90
	Synergy**	26.86	18.66	18.71	46.76	30.77	29.38
Libo-Huanjiang	Trade-off**	0.04	0.00	0.12	0.08	0.00	0.24
	Trade-off*	0.03	0.00	0.02	0.06	0.00	0.02
	Trade-off	10.89	27.11	21.84	22.02	25.28	42.35
	No relationship	0.00	0.00	0.00	0.00	0.00	0.00
	Synergy	0.81	0.71	0.88	1.15	0.89	0.79
	Synergy*	13.67	0.62	0.75	14.64	0.83	0.67
	Synergy**	17.38	14.52	19.20	19.23	30.04	13.12

4. Conclusion

4.1 Driving Factors of ERSs in KWH

Research indicates that SR and CS in KWHs showed an overall increasing trend between 2000 and 2020, while WC declined. Mean SR and WC values in the heritage sites of both study areas exceeded those in their buffer zones, consistent with the findings of Chen et al.'s [20] regarding spatiotemporal variations in ERSs within KWHs. Heritage sites in KWHs are strictly protected, with intact forest structures, high vegetation coverage (Bai et al., 2024), and robust root systems that enhance soil retention capacity. This suppresses erosion and strengthens soil conservation, leading to higher average SR in heritage sites than buffer zones. Additionally, forest communities in heritage sites have greater canopy closure, facilitating rainfall interception for WC. However, their complex vertical structure causes most intercepted rainfall to evaporate. In contrast, buffer zones are dominated by shrublands and grasslands with lower vegetation coverage (Bai et al., 2024); while the reduced transpiration of this vegetation might theoretically enhance WC, actual observations show lower average WC in buffer zones. This is likely due to the deep humus layer and extensive underground root network developed by forest ecosystems in heritage sites over time, which have strong water retention capacity to offset canopy interception effects, maintaining higher WC in heritage sites. For CS, forest age-class structure directly affects sequestration potential (Leng et al., 2024). Young (≤15 years) and middle-aged (16–50 years) forests grow rapidly, accumulate substantial biomass, and have higher CS rates—for example, tropical secondary forests have much higher above-ground biomass growth rates than old-growth forests. Mature forests (>50 years) have slowed growth, stabilized biomass levels, and balanced carbon uptake and release, resulting in lower CS rates (Leng et al., 2024). Heritage sites experience minimal human disturbance, allowing natural forest succession with intact age structures (dominated by middle-aged and mature forests) that support higher overall CS capacity. Buffer zones, however, are influenced by natural and anthropogenic factors (Zhang et al., 2023), often consisting of secondary forests or artificially restored vegetation dominated by young-to-middle-aged forests with rapid growth and elevated CS rates. Thus, buffer zones have higher average CS than heritage sites; although heritage sites hold an advantage in long-term accumulated carbon stocks. Analysis of hotspots and coldspots showed ERS hotspots and coldspots were predominantly clustered in buffer zones, with Shibing showing the most pronounced spatial pattern in WC capacity. The proportions of WC hotspots (11.19%) and coldspots (13.60%) in Shibing's buffer zone significantly exceeded those in its heritage site (3.20% and 4.35%, respectively). Beyond the influences of vegetation types and surface humus discussed in Section 4.1, this disparity is related to spatial variations in rock characteristics and topographic structure. Shibing is dominated by dolomite karst (less soluble than limestone). Its heritage site consists largely of deeply incised gorges with steep terrain that accelerates water runoff, while dolomite's low solubility and fractured nature hinder stable groundwater storage. In contrast, buffer zones are primarily composed of peak clusters and valleys with gentle slopes, facilitating water retention and concentrating higher WC values.

To further validate drivers of ERS spatial differentiation, this study used Geodetector to identify key factors. SR and WC spatial distribution is mainly shaped by topography, while CS is more affected by climate. As the basis of landscape patterns, topography exerts long-term substantial impacts on ERS functions in karst regions with diverse microtopographies. For example, low-lying karst features (caves, subterranean rivers) readily accumulate water. Meanwhile, dissolution-driven landscape evolution concentrates soil in microtopographies like depressions or rock fissures, causing uneven soil thickness that impairs KWHs' soil conservation stability. In addition, vegetation types and species composition vary vary with altitude (Hu et al., 2024); karst depressions and peak clusters, for instance, significantly affect species diversity, thereby influencing WC and SR. Among climatic factors, precipitation and temperature strongly impact CS. In karst regions, water infiltrates underground rivers via expanded fissures, cracks, and conduits in weathered bedrock, making them more rainfall-sensitive than non-karst areas (Luo et al., 2024). Increased rainfall exacerbates surface erosion, inhibiting forest carbon sequestration. However, high plant diversity in karst heritage sites enhances soil roughness and stability, mitigating erosion. This reduces erosion-related carbon loss, weakening rainfall's inhibitory effect on CS (Deng et al., 2019). Temperature affects CS efficiency in two ways. Within optimal ranges, key woody tissue differentiation stages (cell enlargement, wall thickening, maturation) occur earlier, enabling earlier, longer growing seasons. This increases xylem cell formation and radial growth (Stinziano & Way, 2014). Since radial growth is the primary carbon sequestration mechanism, enhanced growth boosts tree carbon storage, strengthening karst forest CS capacity. Conversely, temperatures exceeding optimal ranges harm CS: elevated temperatures accelerate vegetative maintenance and soil heterotrophic respiration, increasing carbon release and reducing CS (Leng et al., 2024).

4.2 Trade-off Synergies in ERSs of KWH

The identification of ERS trade-offs and synergies depends on analytical perspectives and quantitative methods (Li et al., 2024). This study reveals a critical paradox: while the overall average SR across the study area increased significantly from 2000 to 2020, the overall average WC declined slightly, suggesting a trade-off at the macro-statistical scale. However, pixel-based Spearman and partial correlation analyses demonstrated a synergistic relationship between the two services. We classified the study area into synergy zones and trade-off zones based on the directional consistency of WC and SR changes at the pixel scale, and quantified the magnitude of service changes and their areal proportions in each zone (Table 6). Spatial heterogeneity plays a decisive role in shaping aggregate trends. Excluding unchanged areas, Shibing exhibited the largest proportion of simultaneously increasing SR and WC within synergy zones (30.95%), whereas Libo-Huanjiang showed the highest proportion of simultaneously decreasing services in synergy zones (29.75%). This pervasive spatial pattern of directional consistency directly accounts for the synergistic relationship identified through pixel-scale statistical analysis. Furthermore, the gains from SR-increasing pixels (particularly those with high growth rates) in Shibing and Libo-Huanjiang effectively compensated for losses from SR-decreasing

pixels. Conversely, the substantial reductions in WC-decreasing pixels (especially those with high loss rates) outweighed gains from WC-increasing pixels, ultimately resulting in decreased overall average WC alongside increased overall average SR across the study area. “Local drastic changes dominate aggregate trends” constitutes the key mechanism explaining the coexistence of macro-scale trade-off trends and pixel-scale synergy-dominated patterns (Qu et al., 2024). Integrating pixel-scale spatial heterogeneity, directional correlation of changes, and intensity contributions (Zhao et al., 2024) is essential for accurately revealing the intrinsic relationships among ERSs in KWHs.

In terms of temporal variation, WC-CS trade-off values consistently exceeded those of SR-CS, indicating stronger competition between CS and WC and relatively stronger synergies between CS and SR. As discussed in Section 4.1, enhanced forest CS increases vegetation transpiration and canopy interception, reducing rainfall’s soil erosive force and mitigating negative impacts on SR. However, expanded vegetation cover raises water consumption, decreasing water for groundwater recharge and surface runoff, thereby reducing KWHs’ WC capacity and intensifying the WC-CS trade-off—highlighting water resources’ critical role. Notable regional differences exist in the WC-SR relationship: Shibing’s correlation coefficient remained stable (0.21–0.28), while Libo-Huanjiang’s fluctuated more widely (0.39–0.52). This may link to vegetation and topographic differences—complex karst terrain regulates soil depth, slope, and lithology, shaping a non-linear WC-SR relationship [34]. Additionally, Libo-Huanjiang’s WC-CS correlation coefficient increased steadily (from 0.27 in 2000 to 0.46 in 2020), potentially reflecting greater vegetation water demand under climate change, a trend less obvious in Shibing. Both areas showed weak negative SR-CS correlations (Shibing: 0.069–0.29; Libo-Huanjiang: 0.16–0.30), with no significant competition—consistent with previous research on potential weak SR-CS synergy in specific ecosystems. This may stem from vegetation restoration increasing soil organic matter and root SR capacity (Wang et al., 2025), and karst regions’ unique dual-layer hydrological structure differentiating erosion processes (He et al., 2024). In spatial variation, Shibing’s buffer zone has stronger synergies than its heritage site, driven by natural and anthropogenic factors. Compared to the strictly protected heritage site, the buffer zone is more open, with higher connectivity to surrounding ecosystems (Zhang et al., 2023). Frequent material-energy exchange and high biodiversity in the KWH ecological transition zone (Gong, Yin, & Chen, 2023) facilitate mutual enhancement among ERSs. Moderate human interventions (e.g., vegetation restoration, tourism management) and controlled activity pressure can also boost ecosystem self-regulation and service synergies. Libo-Huanjiang’s heritage site and buffer zone show distinct ERS synergy-trade-off patterns, partly due to geological, topographic, and microclimatic differences: the heritage site’s intact landform and stable microclimate sustain synergies, while the buffer zone’s fragmented terrain and unstable microclimate exacerbate trade-offs (Feng et al., 2024). Conservation policies and human activities also play important roles (Chen et al., 2024): strict protection preserves natural synergies in the heritage site, while the buffer zone’s lenient policies and diverse activities (agriculture, tourism) can either enhance synergies or trigger trade-offs, leading to regional and functional zoning characteristics in ERS

relationships.

Table 6. Spatial Proportion Statistics of Ecosystem Regulating Service Change rates(%)

Zone type	Trend of change	Shinbing		Libo-Huanjiang	
		WC	SR	WC	SR
Synergy zone	Decline	2.86	24.35	29.75	24.06
	Increase	24.35	30.95	0.38	8.77
	Unchanged	22.79	12.87	19.87	17.17
Trade-off zone	Decline	2.24	1.22	13.31	6.87
	Increase	6.96	10.47	0.83	9.23
	Unchanged	40.79	38.31	35.86	33.91

4.3 Implications for Ecosystem Management in KWH

The heritage sites have developed unique geographical environments shaped by their complex geomorphology. These environments foster tight coupling between surface water and groundwater, as well as among vegetation, soil, and bedrock—endowing heritage sites with strong self-regulatory capacity. As a result, these areas possess both resistance stability (the ability to withstand external disturbances) and resilience stability (the capacity for self-repair). Heritage sites also benefit from strict policy protections, with large-scale agricultural development, urbanization, and industrial activities strictly prohibited (Zhao, Xiong, & Zhang, 2024). This not only minimizes human-induced conflicts between ecosystem services but also reduces anthropogenic interference with ESs within heritage sites, enabling effective conservation to a large extent. However, despite strong ERS synergies in heritage sites, weaker trade-offs require attention: weakly significant trade-offs (WC-CS and SR-WC) accounted from 16.31% to 27.84%. Though low-intensity, these trade-offs, combined with fragile karst landscapes, may indirectly increase rocky desertification risk, trigger water scarcity, and reduce ecosystem stability (Chen et al., 2024), threatening the OUV of KWHs. To safeguard the authenticity of heritage sites and integrity, we recommend refining KWH monitoring systems—establishing long-term OUV-specific indicators (e.g., vegetation cover, water quality, soil erosion potential)—and developing accurate predictive models. Integrating targeted measures with indicator monitoring will provide robust data for conservation decisions. Natural heritage integrity includes not only in-site OUV but also surrounding environmental coherence. While heritage sites have high SR and WC capacities, their overall ERS capacity is limited: average CS is lower than in buffer zones, with CS hotspots more concentrated there. Higher buffer zone CS highlights their role in addressing climate change and enhancing KWHs' carbon sink function (Leng et al., 2024). Meanwhile, buffer zones have lower average SR than heritage sites, indicating higher erosion risks. As ecological barriers, neglecting buffer zone management could undermine the ecological integrity of heritage sites (Fang et al., 2024). Thus,

buffer zones should be prioritized in unified management frameworks balancing protection and community development needs.

This paper proposes management recommendations for the buffer zones of KWHs by integrating the characteristics of hotspot and coldspot areas with the trade-off and synergy relationships between ERSs. In hotspot zones, conservation should be prioritized in synergistic areas by prohibiting destructive developments such as mining and large-scale tourism infrastructure, while limiting the intensity of human activities. In trade-off zones, the baseline principle of "not compromising the integrity of heritage sites" should be maintained by restricting visitor routes or daily visitor capacity, adopting eco-friendly facilities, and satisfying limited tourism demand without undermining the protective function of hotspot zones for heritage sites. In coldspot zones, synergistic areas should adopt a karst-specific restoration pathway: "soil stabilisation, vegetation establishment, then functional recovery". This entails first securing the soil to prevent erosion, thereby providing a stable foundation for vegetation growth. Subsequently, vegetation restoration should be carried out, with plant growth further consolidating the soil and improving its quality. Finally, ecological functions are enhanced through increased vegetation coverage and ecosystem restoration, achieving the goal of coldspot zone improvement. In trade-off zones within coldspot areas, land use adjustments can transform "destructive trade-offs" into "sustainable synergies". In areas with no significant changes, synergistic zones may moderately enhance service synergies without compromising ecosystem stability, incorporating prior research findings and local conditions. Trade-off zones should establish critical thresholds for service trade-offs through long-term monitoring, and control the intensity of human activities to prevent excessive disturbance.

This study evaluated the spatiotemporal variations and interrelationships of ERSs in KWHs, identified their driving factors, and revealed their trade-off/synergy dynamics, yet it has some limitations. In the ES modeling process, national default parameters were mainly used for factor calculation, which cannot fully reflect the unique topographic and soil characteristics of KWHs. Although parameters were adjusted using previous empirical values, potential uncertainties may still exist in ERS estimations. Future studies should strengthen localized parameter validation by establishing long-term monitoring plots. The systematic collection of key parameters (soil bulk density, rock exposure rate, and water-holding capacity of vegetation litter), combined with high-resolution remote sensing data to improve vegetation cover estimation, will help reduce errors caused by parameterization.

5. Conclusions

This study employed the InVEST model and mathematical empirical models to assess spatiotemporal dynamics of three ERSs—WC, SR, and CS—in KWHs, clarifying their drivers and trade-off/synergy relationships. From 2000 to 2020, SR increased in Shibing but fluctuated downward in Libo-Huanjiang, while WC declined in both areas. Spatially, Shibing exhibited a northwest-to-southeast gradient of decreasing WC and SR and an opposite gradient for CS; Libo-Huanjiang showed consistently higher

WC, SR and CS in the west than in the east. Across the two KWHs, mean WC and SR were higher in heritage sites than in their buffer zones, whereas mean CS was lower. The primary drivers of ERSs in Shibing were slope, DEM, and AT, while in Libo-Huanjiang they were slope, BD, and AF. WC and SR exhibited synergistic relationships, with buffer zones demonstrating higher synergistic contributions. SR and CS, as well as WC and CS, present trade-off relationships. Synergistic effects are stronger in the buffer zones of Shibing, whereas synergistic interactions are more pronounced in the heritage sites of Libo-Huanjiang. Based on these findings, a dual-zone regulatory framework linking heritage and buffer zones was developed to manage ERS trade-offs/synergies, providing a scientific basis for KWH management. Future research should focus on: enhancing long-term monitoring and optimizing parameter inversion with high-resolution remote sensing to improve ERS assessment accuracy; and investigating climate change impacts on KWHs, including ERS mechanisms and trade-off/synergy evolution under different scenarios, to lay a foundation for climate-resilient conservation strategies.

References

Costanza, R. et al. (1997). The value of the world's ecosystem services and natural capital. *nature*, *387*(6630), 253-260.

Zhang, S. et al. (2021). Evolution and determinants of ecosystem services: Insights from South China karst. *Ecological Indicators*, *133*, 13.

Carpenter, S. R., Bennett, E. M., & Peterson, G. D. (2006). Scenarios for ecosystem services: An overview. *Ecology and Society*, *11*(1).

Fang, R. et al. (2024). Integration of the Natural World Heritage conservation and development of buffer zone agroforestry: From scientometrics insights and implications for the Karst World Heritage. *Heritage Science*, *12*(1), 21.

Zhang, M. et al. (2022). Natural Beauty and Esthetic Value of Natural World Heritage Sites: a Literature Review and Implications for Karst Geoheritage Sites. *Geoheritage*, *14*(3).

UNESCO World Heritage Centre, Operational Guidelines for the Implementation of the World Heritage Convention. (WHC.21/01). Paris: UNESCO.

Zhao, X., Xiong, K., & Zhang, M. (2024). Advances and prospect in natural beauty evaluation: Insights for the World Heritage karst. *Heritage Science*, *12*(1), 21.

Huang, S. et al. (2024). Spatiotemporal changes and driving mechanism of ecosystem carbon sink in karst peak cluster depression basin in Southwest Guangxi based on the interaction of "water-rock-soil-air-biology". *Ecological Informatics*, *83*, 17.

Liu, Y., Lian, J., & Chen, H. (2024). Assessment of the restoration potential for ecological sustainability in the Xijiang River basin, Southwest China: A comparative analysis of karst and non-karst areas. *Science of the Total Environment*, *912*, 9.

Xiong, K., Li, G., & Wang, L. (2012). Study on the protection and sustainable development of South China Karst Libo world natural heritage site. *Chin Gard*, *28*(08), 66-71.

He, G., Zhao, X., & Yu, M. (2021). Exploring the multiple disturbances of karst landscape in Guilin World Heritage Site, China. *Catena*, *203*, 11.

Gong, T., Yin, X., & Chen, H. (2023). Soil oribatid mite community structure and its relationship with environmental factors in different agricultural land-use types in Shibing Karst. *Environmental Research Communications*, *5*(11), 18.

Chang, Y., Zhang, Z., & Yao, C. (2026). Exploring the Multiscale Spatiotemporal Dynamics of Ecosystem Service Interactions and Their Driving Factors in the Taihu Lake Basin, China. *Sustainability*, *18*(6), 2930.

Zhang, X. et al. (2025). Trade-Offs and Synergies of Ecosystem Services and Their Driving Factors on the Northern and Southern Slopes of the Nanling Mountains. *Forests*, *16*(11), 1634.

Wang, J. et al. (2024). Exploring the complex trade-offs and synergies of global ecosystem services. *Environmental Science and Ecotechnology*, *21*, 100391.

Xia, T., & Huang, J. (2025). Assessing Synergistic Effects on NPP from a Refined Vegetation Perspective: Ecological Projects and Climate in Heilongjiang. *Forests*, *16*(10), 1574.

Jiang, W. et al. (2025). Quantifying impacts of climate and land use changes on ecosystem services from statistic perspective. *Ecological Indicators*, *172*, 113285.

Zhang, J. et al. (2024). Exploring the synergy between Karst World Heritage site's OUV conservation and buffer zone's tourism industry development: A case study of the Libo-Huanjiang Karst. *Heritage Science*, *11*(1), 19.

Bai, X. et al. (2024). Spatiotemporal evolution of landscape stability in World Heritage Karst Sites: a case study of Shibing Karst and Libo-Huanjiang Karst. *Heritage Science*, 12(1), 20.

Chen, Y. et al. (2024). Spatiotemporal changes and driving factors of ecosystem services between karst and non-karst World Heritage sites in Southwest China. *Heritage Science*, *12*(1), 278.

Feng, M. et al. (2024). The Temporal Variation and Spatial Scale Dependence of the Trade-Offs and Synergies among Multiple Ecosystem Services in the World Heritage Site of South China Karst. *Land*, *13*(9).

He, L. et al. (2024). Exploring the interrelations and driving factors among typical ecosystem services in the Yangtze river economic Belt, China. *Journal of Environmental Management*, *351*.

Li, Q. et al. (2024). Trade-offs and synergies of ecosystem services in karst multi-mountainous cities. *Ecological Indicators*, *159*.

Leng et al. (2024). Forest aging limits future carbon sink in China. *One Earth*, *7*(5), 822-834.

Zhao, Z., & Shen, Y. (2022). Rain-induced weathering dissolution of limestone and implications for the soil sinking-rock outcrops emergence mechanism at the karst surface: A case study in southwestern China. *Carbonates and Evaporites*, *37*(4).

Hu, G. et al. (2024). Beta Diversity Patterns and Determinants among Vertical Layers of Tropical Seasonal Rainforest in Karst Peak-Cluster Depressions. *Forests*, *15*(2).

Luo, D. et al. (2024). Evolution and driver analysis of forest carbon stocks in karst mountainous areas of southwest China in the context of rocky desertification management. *Catena*, *246*, 16.

Deng, L. et al. (2019). Land-use changes driven by "Grain for Green" program reduced carbon loss induced by soil erosion on the Loess Plateau of China. *Global and Planetary Change*, *177*, 101-115.

Stinziano, J. R., & Way, D. A. (2014). Combined effects of rising [CO2] and temperature on boreal forests: growth, physiology and limitations. *Botany*, *92*(6), 425-436.

Leng, Y. et al. (2024). Forest aging limits future carbon sink in China. *One Earth*, *7*(5), 822-834.

Li, Q. et al. (2024). Trade-offs and synergies of ecosystem services in karst multi-mountainous cities. *Ecological Indicators*, *159*, 111637.

Qu, S. et al. (2024). Spatial–temporal evolution and driving factors of ecosystem services trade-offs and synergies in karst areas from a geospatial perspective. Land Degradation & Development, *35*(10), 3448-3460.

Zhao, M. et al. (2024). *Threshold Effects between Ecosystem Services and Natural and Social Drivers in Karst Landscapes*. *Land*, *13*, 691.

Wang, F. et al. (2024). The nonlinear rainfall–quick flow relationships in a humid mountainous area: Roles of soil thickness and forest type. *Journal of Hydrology*, *641*.

Wang, S. et al. (2025). Vegetation restoration shapes soil organic matter chemistry and microbial processes. *Soil Biology & Biochemistry*, *211*, 16.